Artificial Intelligence Identification of Multiple Microfossils from the Cambrian Kuanchuanpu Formation in Southern Shaanxi, China

ZHANG Tao[1, 2], WANG Bin[1, *], LI Dedong[1], NIU Ben[1], SUN Jie[2], SUN Yifei[2], YANG Xiaoguang[2, *], LUO Juan[2] and HAN Jian[2]

[1] *School of Information Science & Technology, Northwest University. Chang'an District, Xi'an 710075, China.*
[2] *Shaanxi Key Laboratory of Early Life and Environmensts, State Key Laboratory of Continental Dynamics, Department of Geology, Northwest University, Xi'an 710069, China.*

Abstract: The Cambrian Kuanchuanpu Formation in southern Shaanxi, China is a critical window for the understanding of the Cambrian explosion, because of abundant and various exceptionally preserved metazoans and embryo fossils yielded. The efficiency of traditional sample manually selecting with microscopes is quite low and hinder the discoveries of new species, thus recognition and classification of microfossils by artificial intelligence (AI) is substantially in the request. In this paper, we develop a procedure for fossil area segmentation in common multi-typed mixed photos by improved watershed algorithm. And for better fossil recognition, previous histogram of oriented grandient (HOG) algorithm is replaced by scale invariant feature transform (SIFT), which is feasible for the segmented images and increase the accuracy significantly. Thus, the scope of application of AI fossil recognition can be extended form single fossil image to multi-typed mixed images and the reliability is also secured, as the result of our test presents a high (at least 84%) accuracy of fossil recognition.

Key words: watershed segmentation, scale invariant feature transform, visual vocabulary, support vector machine

Citation: Zhang et al., 2020. Artificial Intelligence Identification of Multiple Microfossils from the Cambrian Kuanchuanpu Formation in Southern Shaanxi, China. Acta Geologica Sinica (English Edition), 94(1): 189–197. DOI: 10.1111/1755-6724.14498

1 Introduction

The Cambrian Kuanchuanpu Formation in southern Shaanxi, China, ca. 535 Million years ago, has been well known for its three-dimensional preservation of various microscopic metazoans and embryo fossils (Qian, 1977; Han et al., 2017). Although simple in appearance, the microfossils from the Kuanchuanpu Formation have been a critical window for the understanding of the Cambrian explosion and the origin of phyla due to soft-bodied preservation (Han et al., 2017; Yang and Han, 2017). Hitherto, a wide scope of fossil associations, including cyanobacteria (Zheng et al., 2017), algae (Liu et al., 2014), possible protists (Zhang et al., 2017), nine animal phyla (Steiner et al., 2004a; Zhang and Dong, 2015; Zhang et al., 2015), and many problematic forms (Steiner et al., 2004a) organisms have been found from this formation. Traditionally, finding new taxa among numerous microfossil specimens is time-consuming and labor costing, and it became lower efficient after more than 40 years of research as the gradual addition of the species menus. All-new taxon (Liu et al., 2017) in recent years and in the future have been proven very rare . While taking advantage of stable morphological profiles and extremely abundance of these microfossils, it is possible to adopt artificial intelligence to recognize and select target microfossils. Recently we have succeeded in dealing with the simplest case: to test manually isolated single specimen by developing a multicategory fossil recognizer based on support vector machine (SVM) (Zhang et al., 2019). But a more common complicated case is multi-type mixed image, which means one image acquired under microscope frequently contains several microfossils that are separated from each other or being attached together. In this circumstance, we develop a new procedure of accurate image segmentation and an improved fossil recognition method ensuring a high accuracy of fossil recognition.

2 Geological Settings

All the fossils materials for AI test were collected from are found in phosphatic limestone, belonging to Lower Cambrian Kuanchuanpu Formation in Hexi Section, Xixiang County, Shaanxi Province. The Kuanchuanpu Formation is separated by an unconformity from the underlying dolostone of Ediacaran Dengying Formation and underlies disconformably the Lower Cambrian Guojiaba Formation of black shale (Fig. 1b). The age of sampling horizon is estimated as 535 Ma, belongs to the

* Corresponding author. E-mail: wbin@nwu.edu.cn, lqzy0301@gmail.com

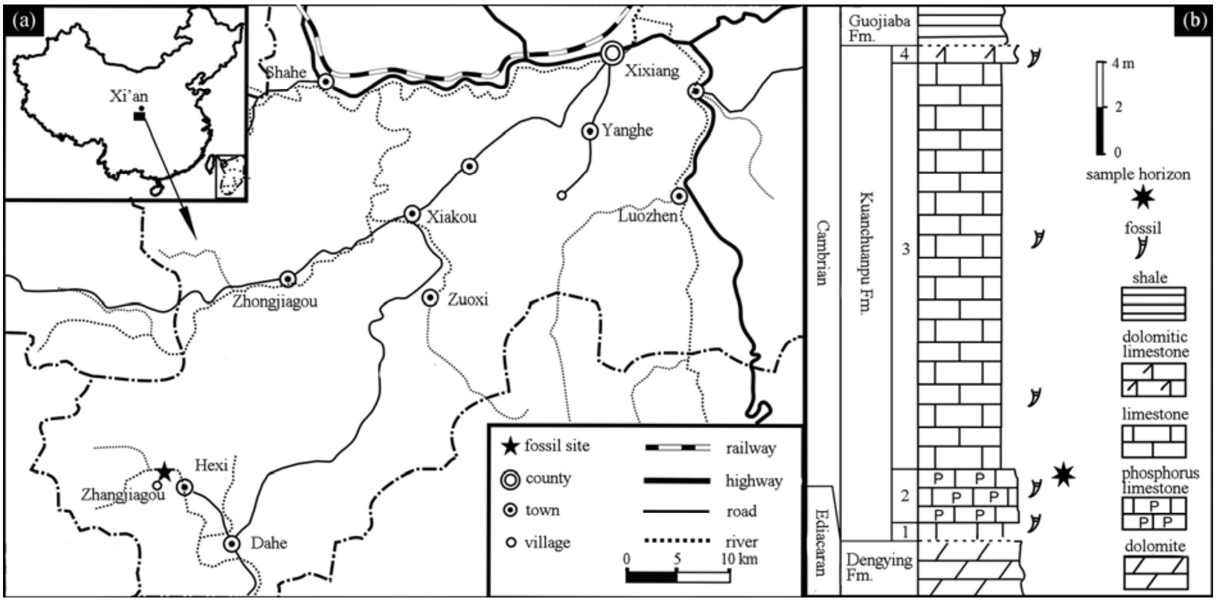

Fig. 1. The locality (modified from Han et al., 2017b) and stratigraphic column (modified from modified from Yang et al., 2017) of Kuanchuanpu Fomation in Xixiang, Shaanxi, China.

Fortunian Stage, Terreneuvian Series (Peng et al., 2012), since the micro fossils can be comparable with the *Anabarites trisulcatus-Protohertzina anabarica* assemblage zone and different from spatiotemporally contiguous Ediacaran microfossils assemblages, such as *Sinotubulites* and *Cloudina* (Steiner et al., 2007, 2014; Gu et al., 2018).

3 Materials and Methods

The rock samples were treated with 8%~10% acetic acid solution, with the insoluble remains being examined with microscopes.

The fossils were photographed by a Leica M205C microscope with a Leica LED5000HDI light source and a NatureGene ProgRes C3 CCD. All the fossils images were taken under uniform brightness and magnification (×10). The original image resolution is 2592×1944 in pixel, then the resolution was converted into 800×600 for later digital process. A blue background is used to enhance the contrast with white or black microfossils. Hardware and software environment for all the tests and analyses was based on DELL T7600 graphical workstation, with Windows 10 OS and Python 3.6 for algorithmic design and development.

We have acquired more than 5000 images in total and those with good quality were selected. The number of images for AI training and testing is 615 and 150 respectively. In initial stage, all fossils materials were divided into 3 types: tubular fossils, spherical fossils and dross. We chose 205 images of each types to construct training set. These images only contained single fossil. On the other hand, we chose 100 images of mix-type fossils, then used segmentation algorithm (see in 5.1) to achieved hundreds of images of each type. We selected 150 images (50 of each type) form them as the final testing set.

4 Paleontological Background and Requirements Analysis

4.1 The characteristics of target fossils

This program focusses on the microfossils form early Cambrian, which have been intensively studied for decades.The dominant morphology types of all fossils are tubular and spherical ones.

The Genus *Conotheca* and *Anabarites* are the most common tubular components of this fossil assemblage. *Conotheca* are small conical tubes with circular cross-section and blunt terminations. The conch surfaces are almost smooth, except for some weak growth lines parallel the aperture (Fig.2b). *Anabarites* are similar elongate cones while the cross-sections are tri-radial. Accordingly, each tube is divided into 3 lobes by 3 longitudinal sulci. Some species have similar conch surfaces as *Conotheca*, while some possess prominent transverse ridges. Protoconodonts can also be assigned into tubular type approximately. These fossils are abundant and key elements among many of the earliest skeletal faunas and Genus *Protohertzina* is the commonest kind. *Protohertzina* are tiny and gently curved spines, which is much slenderer than those tubes mentioned above. The strongest curvature occurs on distal part, whereas the proximal part is almost straight. The cross-sections are teardrop-shaped, with two shoulders formed by posterolateral ridges (Fig. 2c). Some other fossil taxa also appear as general tubular shape, including *Hyolithellus, Siphogonuchites, Rhabdochites* and *Lopochites* (Bengtson et al., 1990; Steiner et al., 2004a).

Most of the spherical ones are embryo fossils (Fig. 2d). Those embryos belong to varied taxa with different surface textures and ornaments. The most common *Olivooides* late embryos show pentaradial symmetry in oral part, some holoblastic cleavage embryos in the early

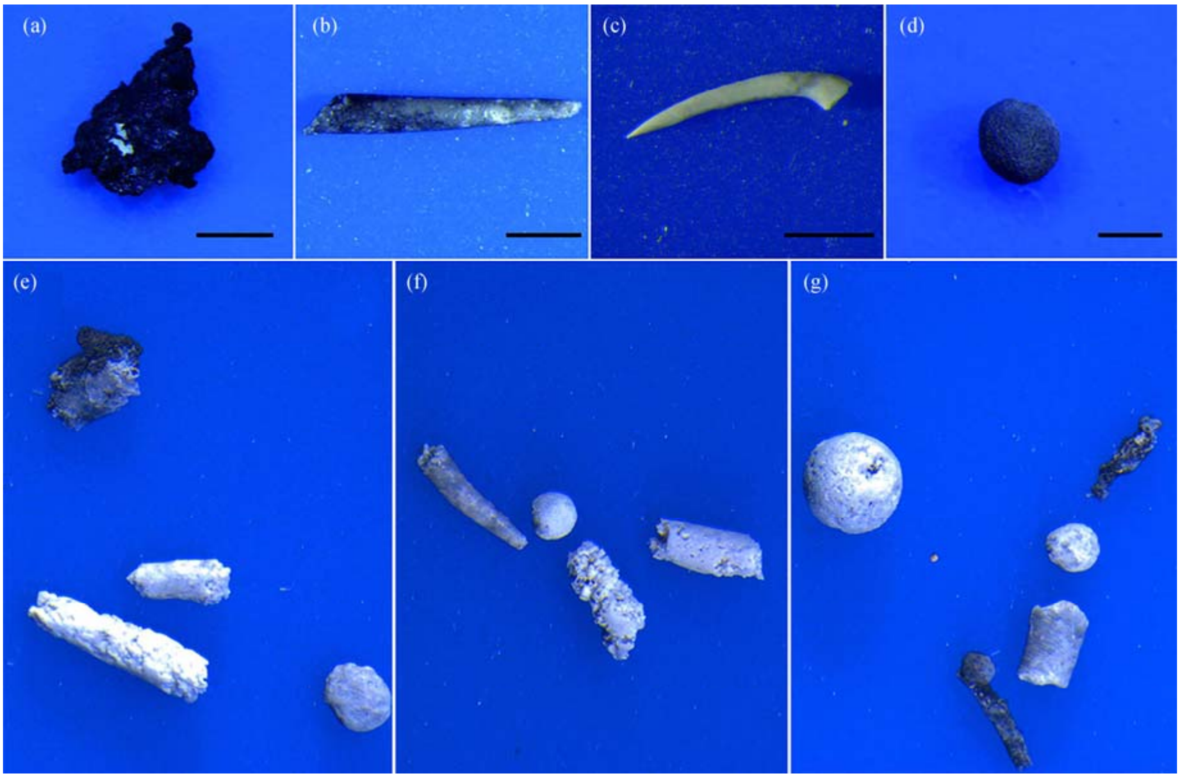

Fig. 2. Fossil image acquisition in different strategies.
(a-d) Single fossil images; (a) dross particle; (b) *Conotheca*; (c) *Protohertzina*; (d) Embryo fossil; (e-g) Multi-type mixed images. (Scale bar: 1 mm)

blastula stage show confined blastomeres clearly, while some embryos are covered by intact envelope and appear as smooth spheres. Although the internal structures of these spherical fossils vary dramatically, their general external form is distinguishable. Other fossils may form spheres in less regular shape, such as colonies of algae or bacteria (Steiner et al., 2004a, 2004b; Han et al., 2013, 2016).

4.2 Function requirements

The system of AI fossil identification comprises of software and hardware. The key function of hardware would include transportation of unselected samples, image acquisition and partition of targets by fossil types. In this initial stage, our hardware system could transport samples and spread them on a small platform for image acquisition (see supplement). Based on the images acquired, we can design algorithm of fossil identification. Those identified specimens will be picked up and moved into different storages by a new mechanical part, which is still under developing.

In previous study (Zhang et al., 2019), we already developed a prototype, using single fossil images which are deliberately selected by human (Fig. 2a–d), for the test the feasibility of AI fossil identification. Although the result is promising, this prototype is only theoretical. In order to put it into practice, two essential functions are needed:

(1) The ability of dealing with multi-type mixed images with different taxa of microfossils and debris. In normal circumstance, what obtained by human eyes during sample selecting are such mixed images. In our system, the mechanical part will spread some raw samples on a small platform for image acquisition (Fig. 2e–g), simply simulating this process. Then the software needs to separate each fossil or dross from the original images.

(2) Identifying and classifying targets into different categories based on fossil features. For a quick and primary application, we set 3 categories: tubular fossils, spherical fossils and dross. It will also maximize the practicality of this system in paleontological research, since tubular and spherical types cover a substantial portion of fossil materials.

5 Algorithm Design and Execution

5.1 Image segmentation

As our new requirement, the first step is segmenting single targets from the multi-type mixed images. Watershed algorithm is the most common approach and the main steps are as follow (Fig. 3):

5.1.1 Image binarization and morphological operation of s component

For accuracy, all the images for AI recognition need to be converted into HSV (hue-saturation-value) color space images, then binarizing them with the S component by threshold segmentation method defined in formula 1. S(x, y) represents the value of S component image at coordinates (x, y) and th correspond threshold of binarization. Comparing the value of each pixel in the S component image with the threshold value, if S(x, y)≥th, value in the coordinate position is reset to 1, otherwise it is reset to 0, thus realizing binarization.

$$S(x,y)=\begin{cases}1 & S(x,y)\geq th\\ 0 & S(x,y)<th\end{cases} \tag{1}$$

Then mean shift filter algorithm was applied to perform image smoothing processing. In the filter, the offset radius of physical space is 10 pixels, the offset radius of colour space is 100 (number range from 0 to 255). After that, smaller noise points within fossil areas need to be dealt with by opening and closing operation in the binary S-component image. The opening operation in mathematical morphology (defined as Formula 2:

A represents S component image after binarization, B represents structural image of morphological operation, the structuring element of B is a 3×3 matrix, $\ominus$ represents erosion operation and $\oplus$ represents dilatation operation) means to perform erosion operation with B and A first, and then use dilatation operation with B and A (Gonzalez and Woods, 2008). The result of opening operation is removing small noise points in binary image. Meanwhile, the closing operation (defined as Formula 3) is to fill the void in the fossil area by using dilatation operation with B and S first and then use erosion operation with B and S.

$$A\circ B=(S\ominus B)\oplus B \tag{2}$$

$$A\bullet B=(S\oplus B)\ominus B \tag{3}$$

5.1.2 Distance transformation and completing the segmentation

In the binary image, taking the four neighborhoods of the central pixel as an example: if the central pixel is a pixel value of 1 and the surrounding four neighborhoods are all pixel value of 1, then the point is denoted the internal point. If the central pixel is a pixel value of 1 and the surrounding four neighborhoods are all pixel value of 0, the central point is denoted isolated point (Malik et al., 2001).

Distance transformation is to obtain the set of all internal points that denoted S_1 and the set of non-internal points that denoted S_2 in the binary image at first; then, for each interior point P(x, y) in S_1, the minimum distance between P and points in S_2 is calculated by distance formula 4, and the minimum distance is formed into a set D_1; finally, the maximum D_{max} and minimum D_{min} values in D_1 are obtained, and the gray value (G) of each internal point in the set S_1 is converted by the formula 5(Vincent, 1993). According to the Euclidean distance between each pixel and the surrounding pixels in the binary image, a distance image reflecting the distance between the fossil and the background can be obtained.

$$D=\mathrm{sqrt}[(x-i)^2+(y-j)^2] \tag{4}$$

Where the sqrt denotes square root, (x, y) represents the coordinates of the target pixel, (i, j) represents the

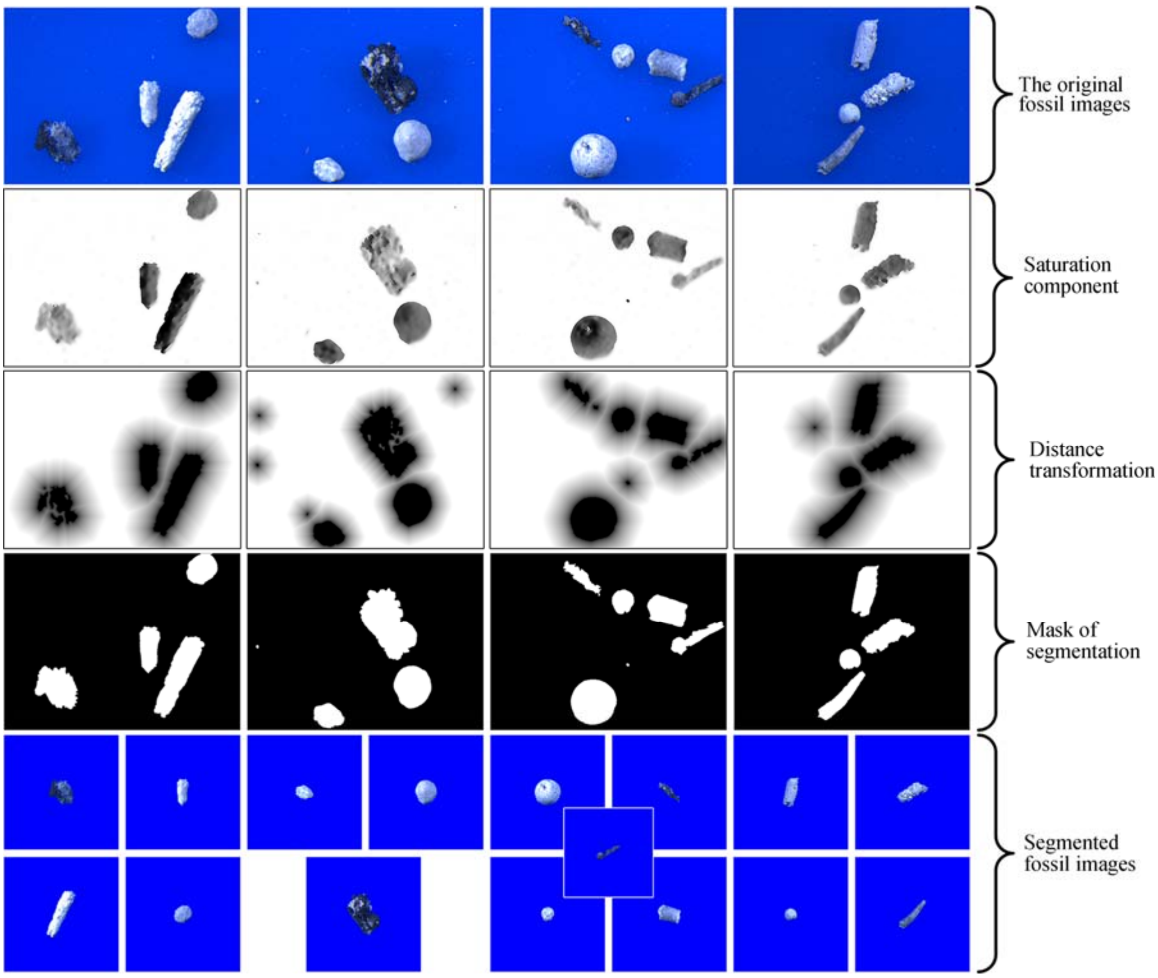

Fig. 3. Watershed segmentation process and results of multi-type mixed fossil images.

coordinates of background pixel.

$$G(x, y)=255\times|D_1(x, y) - D_{min}|/|D_{max} - D_{min}| \quad (5)$$

After distance transformation, In the distance matrix D, those elements with value lager then threshold value will be set as boundaries. The threshold value is determined by formula 6 (d_{ij} represents each element in matrix D). Then the boundaries of each fossil area can be achieved. With these boundaries, the contour information of the fossil is extracted and the segmentation mask can be constructed accordingly, which finally realizes the segmentation and so that each target is extracted from a multi-type mixed image (Fig. 3).

$$th = \left[\max_{i\in m, j\in n} |d_{i,j}| \right] \times 0.994 \quad (6)$$

5.2 Fossil recognition

5.2.1 Feature extraction of fossil images

Segmented images are now processed for recognizing and classifying base on the different features, which can be described by Scale Invariant Feature Transform (SIFT) for a computer. SIFT shows in-variance with rotation, scale and brightness, and resistance of view transformation and image noise (Lindeberg, 2012). Major steps of SIFT analysis are as follows: 1) Space extremum points detection with difference of Gaussians (DoG); 2) Location of SIFT feature points; 3) Direction detection of SIFT feature points; 4) Generation of SIFT feature vectors.

Normally, when an object is observed by human eyes, it can be distinguished regardless of the size changes within a certain range. In order to make the computer achieve similar behavior and extract the features of an object with similar scale-invariant characteristics, it is necessary to provide various object images of different sizes and clarity to the computer for learning. For this reason, the SIFT feature extraction algorithm designs a multi-scale object image DoG pyramid to find SIFT feature points (Fig. 4b) and finally construct a 128-dimensional SIFT feature vector (Fig. 4c) (Mortensen et al., 2005).

5.2.2 SIFT bag of words model of the training set of fossil samples

Due to the difference of perspective, shape, surface texture and the number of feature points in different samples, the bag of words (BoW) model (Zhang et al., 2010) is needed to find the common features of the same type of fossil images and the differences between different types of fossils.

As in Fig. 4, we take three types of the targets as an example, assuming the total amount of fossil training image is n, namely I_1-Source, I_2-Source, … I_n-Source. First, the SIFT features of each image need to be extracted and represent as I_1-SIFT, I_2-SIFT, … I_n-SIFT, then all 128-dimensional feature vectors in each image form a matrix in Fig. 4c, at last, K-Means clustering algorithm (Wagstaff et al., 2001) cluster the column of C and form a new matrix in Fig. 4d, which shall be the visual vocabulary or “codebook”. The clustering process can also be understood as classifying SIFT feature points of all fossil sample images. In this “codebook”, the center of each identified cluster is a single “word”, which represents major feature of each fossil type.

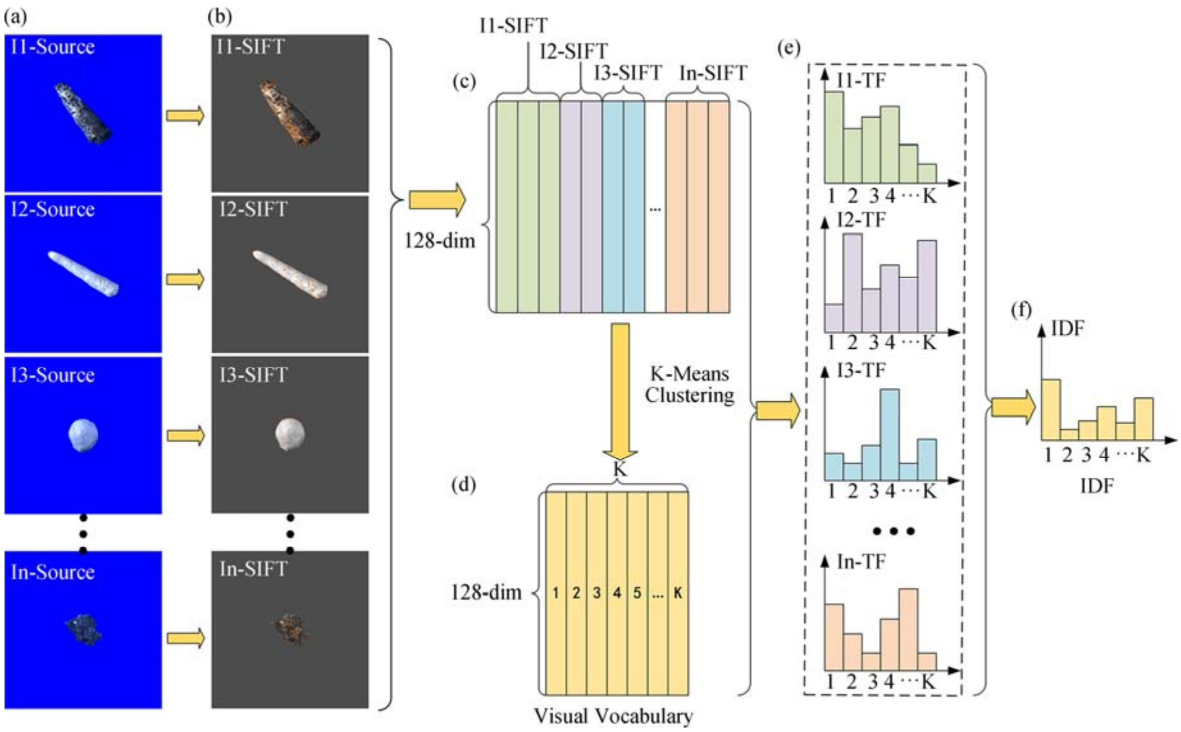

Fig. 4. The process of constructing the SIFT-BoW model (visual vocabulary).
(a) The segmented fossil image list including tubular fossil, spheroidal fossil, residue detritus; (b) the SIFT feature points of fossil images; (c) matrix of SIFT features of all images in the training set; (d) visual vocabulary formed by K-Means clustering; (e) frequency statistic of SIFT features within visual vocabulary of each image (TF); (f) inverse document frequency calculated by accumulating each histogram in C (IDF) .

5.2.3 Inverse Document Frequency Analysis of Bag of Word Model of Fossil Sample Image in Training Set

The technology of term frequency–inverse document frequency (TF-IDF) (Chum et al., 2008), which is mainly used in text data mining, can evaluate the importance of words in a document or a file set in a corpus. This method is mainly divided into two parts: term frequency (TF) statistics and inverse document frequency (IDF). TF mainly counts the occurrence of words in documents, and IDF mainly reflects the occurrence of the file containing particular words among all files.

The idea of the TF-IDF technique can also be applied in the analysis of fossil image features. In this scenario, each SIFT feature point in each fossil sample image is regarded as a word, and the visual vocabulary formed by clustering in SIFT-BoW model is regarded as a document. TF vectors are generated by counting the frequency of SIFT feature points appearing in the visual dictionary of each fossil image. The TF vectors in all fossil images of the training set are accumulated by K clustering centers. Finally, the IDF vectors are calculated by formula 7 and the flow chart of this calculation is shown in Fig.5.

$$\mathrm{IDF}_i = \log[\mathrm{K}/(\mathrm{N}_i + 1)] \quad i=1,2,\ldots,\mathrm{K} \tag{7}$$

The K represents the number of clustering centers in visual vocabulary, the N_i represents the accumulated occurrence in all training set when the clustering centers count to i, IDF_i represents inverse document frequency when the clustering centers count to i. IDF vectors can be generated after the calculation has been performed in all clustering centers.

IDF plays the key role of feature weighting in the representation of fossil image features. According to formula 7, SIFT features with high occurrence (N_i) among all types of fossils in the training set will have low IDF values, while SIFT features with fewer occurrences will have high IDF values. These features of SIFT with high IDF values will be more useful for fossil classification.

5.3 The representation of fossil image features of the training set

Fossil samples in the training set are comprised of many different types. In order to construct the features for learning and training of each type of fossil image, TF-IDF features processing is needed for every type of fossil. The process is shown in Fig. 5 and it can be divided into 3 steps:

(1) SIFT features are extracted from each image of the same type of fossil image (I1, I2, …, In), and a 128×n SIFT feature matrix in (a) is constructed.

(2) Comparing the SIFT features of each image with the visual vocabulary of clustering centers expressed by matrix in (b). Judging the assignment and statistic the number of occurrences of feature points, and finally, the TF histogram vectors of each image will be obtained.

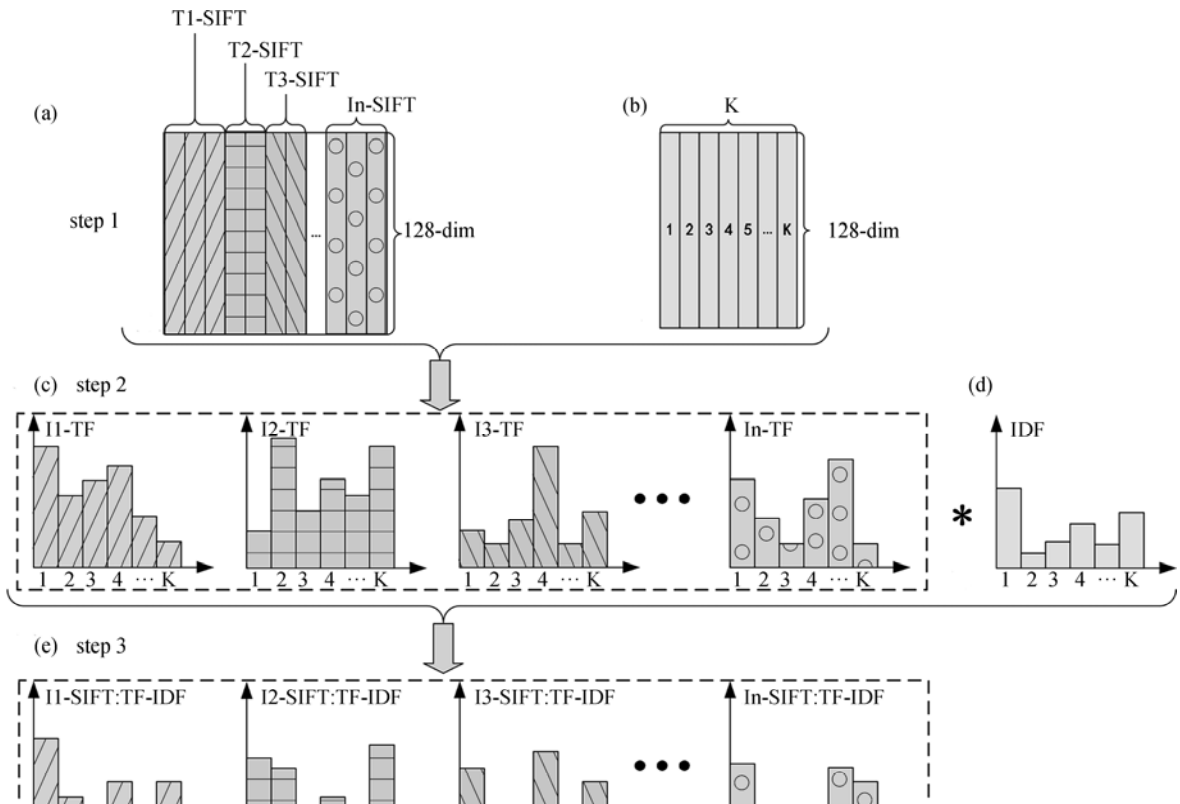

Fig. 5. The feature representation procedures for each type of fossil training set.

(a) The SIFT feature matrix of fossil training set images of the same type. (b) the visual vocabulary based on K-Means clustering of all types of training set images. (c) The TF statistics of similar fossil images. (d) The IDF vectors generated from images of all types of the training set. (e) The TF-IDF obtained by weighting of TF in C graph with IDF in D graph.

(3) The TF histogram of each image in (c) is weighted with IDF histogram one by one, and the weighted corrected TF-IDF is generated.

After the TF-IDF process of SIFT features of fossil images, the representative features of the certain type of fossil images can be better selected.

5.4 Recognition of segmented fossil images

Considering lots of individual fossil images that have been artificially recognized and labeled previously, we use support vector machine (SVM), which is a supervised machine learning method, for fossil classification and recognition. At present, SVM algorithm has been widely used in various fields of data mining, data classification and data recognition (Cortes and Vapnik, 1995; Cusano et al., 2003). The SVM in this paper is almost the same with the one we design formerly (Zhang et al., 2019).

For AI training and learning, each single fossil image that has been labeled artificially is used as a sample in the training set. SIFT features are extracted from each type of single fossil sample and clustered to generate SIFT-BoW model. Then TF-IDF algorithm could find representative feature vectors. Finally, the feature vectors are sent to the SVM classifier. As we know, the fossils are divided into 3 types: tubular, spherical, and dross, so two SVM classifiers need to be trained, namely, SVM1 separate dross from other types, and SVM2 separate spherical and tubular fossils (Abedi et al., 2012; Lee and Lee, 2007; Lindeberg, 2012).

Fig. 6 shows the testing process of identification of multi-types mixed fossil images. Firstly, each image with mixed fossils is segmented into several images with individual fossil by watershed algorithm. Then SIFT features are extracted from each segmented fossil image and TF-IDF processing is performed to generate the recognizable features. Finally, the features are imported into two SVM classifiers of fossils to be discriminated.

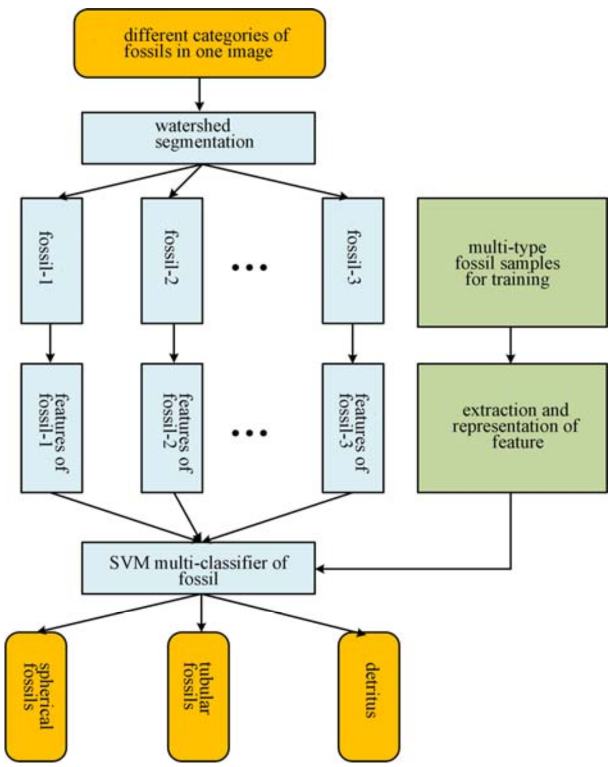

Fig. 6. The process of multi-types mixed fossils identification.

6 Discussion

6.1 Image binarization as preparation of applying watershed algorithm.

The idea of the watershed image segmentation algorithm originates from topography. In an image, the boundaries of different objects and background are considered as virtual ridges between the basins which can segment images like watersheds (Haris et al., 1998). The most commonly used watershed algorithm is the flooding algorithm (Asundi and Wensen, 1998) (Fig. 7).

However, during the image processing, due to equivalence of gray value of the pixels in the image and the elevation of the topographic map, using the original gray value in a common photo will make the algorithm too sensitive to the noise and small gray changes and lead to the over-segmentation that the image region originally belonging to the same object is divided into multiple regions (Beucher, 1994). In order to avoid over-segmentation, the original gray-scale image needs to be converted into the binary image and the method of distance transform is necessary to reflect the distance between the target and the background (Bailey, 2004). After these steps, the watershed algorithm can be eligible to find the boundaries of target areas in a gray-scale image.

6.2 Adoption of S-component for successful segmentation

In most instances, the color photos of fossils are stored and presented by RGB (red-green-blue) color space color space (Süsstrunk et al., 1999). However, the RGB space couldn't distinguish fossils from the blue background very well. Therefore, HSV color space is more appropriate for extracting fossil areas and segmentation, because the three components: H (hue), S (saturation), and V (value) (Cucchiara et al., 2001; Sural et al., 2002) are different attributes of a color image. H is measuring the range of color by angle, S represent the degree of closeness between color in image and spectral color, V define the brightness of color. We need to find which of 3

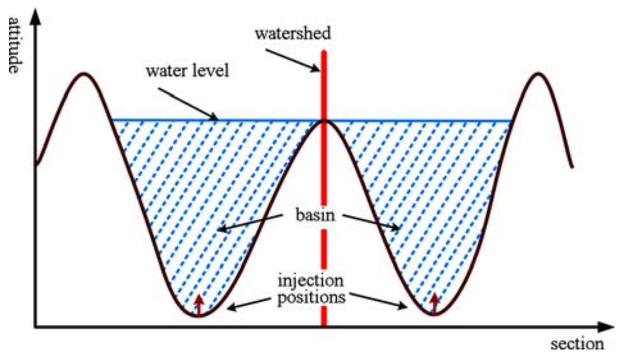

Fig.7. Watershed image segmentation algorithm model

components is the best for distinguishing fossils from background. Base on a random test of 200 fossil images, we extracted all 3 components and made comparisons, the results reveal that image binarization by using S component can better highlight fossils from the background, since in this situation, the difference between background and fossil could be maximized and more integrate fossil area could be extracted accurately. While using H component usually cause incomplete extraction of fossil areas because the difference of blue background and fossil areas are not adequate to distinguish each other, and using V always cause failure for extracting targets, since V component shows almost no difference between background and fossil areas.

6.3 SFIT algorithm for more accurately recognition

Fossil features acquisition is the first step of AI recognition. Previously, this task is completed by the HOG algorithm. the HOG algorithm is a feature algorithm for object edge detection, which can construct features by collecting and computing statistical information of a specific area of an image. When dealing with image which only contain single fossil sample, it could achieve 95% or higher accuracy for fossil recognition, by extracting statistical gradient data as the fossil boundaries (Zhang et al., 2019).

However, when the HOG algorithm is applied to each segmented image form a multi-type mixed photo, the accuracy dropped dramatically to approximate 60%. The reason we assumed is the nature of HOG algorithm is not suitable in this condition. The essential idea of HOG is extracting the gradient in an image, the accuracy depends on the difference of gradient feature. In our experiment, during the segmentation, each target object area (fossil or dross) were extracted and given a new background in the new segmented images, which caused the loss of gradient features along the object edges and lead to the rapidly decreased recognition accuracy. In this paper, after a series of tests of feature extracting algorithm, we finally develop a new model by using SIFT with BoW model to extract and present fossil features, which can effectively avoid the error before and after image segmentation.

7 Conclusion

The results of AI recognition are shown in Table 1. In this experiment, totally 615 images are used for training set. Those images are composed of three types (tubular, spherical, dross, each type 205 images) of selected single fossils sample. While totaly150 images are used as testing set. These images are segmented from multi-type mixed fossil images and classified into three types (tubular, spherical, dross, each type 50 images).

The data demonstrate that: (1) with considerable amount of training, we have achieved at least very high accuracy in identification microfossils, proving a great perspective of AI identification for early Cambrian microfossils. (2) We extend the scope of application of AI recognition form images with single fossil to multi-typed mixed fossil images with microfossils in different types, positions, amounts and postures. (3) We develop reliable approaches for fossil image segmentation by the watershed algorithm, and for more accurate fossil feature extraction under the circumstance of segmented image based on SIFT algorithm rather than HOG algorithm.

Table 1 The recognition results of segmented multi-types mixed fossil images

target types	training amount	testing amount	accuracy	misjudgment rate
dross	205	50	98.0%	2.0%
spherical	205	50	90.0%	10.0%
tubular	205	50	84.0%	16.0%

Acknowledgments

We thank reviewers for their constructive advices and editor H. C. Fei' s work. This work was supported by the Strategic Priority Research Program of Chinese Academy of Sciences [No. XDB26000000] and the Natural Science Foundation of China [Nos. 41621003, 41772010, 41572017, 41672009, 41720104002].

Manuscript received Oct. 29, 2019
accepted Dec. 2, 2019
associate EIC FEI Hongcai
edited by FEI Hongcai

References

Abedi, M., Norouzi, G.H., and Bahroudi, A., 2012. Support vector machine for multi–classification of mineral prospectivity areas. Computers & Geosciences, 46: 272–283.

Asundi, A., and Wensen, Z., 1998. Fast phase-unwrapping algorithm based on a gray–scale mask and flood fill. Applied Optics, 37(23): 5416–5420.

Bailey, D.G., 2004. An efficient Euclidean distance transform. In: International workshop on combinatorial image analysis. Berlin, Heidelberg: Springer, 394–408.

Bengtson, S., Conway Morris, S., Cooper, B.J., Jell, P.A., and Runnergar, B.N., 1990. Early Cambrian fossils from south Australia. Brisbane: Association of Australasian Palaeontologists, 190–213, 330–331.

Bengtson, S., and Yue, Z., 1997. Fossilized metazoan embryos from the earliest Cambrian. Science, 277 (5332): 1645–1648.

Beucher, S., 1994. Watershed, hierarchical segmentation and waterfall algorithm. In: Serra, J., and Soille, P.(eds.), Mathematical Morphology and Its Applications to Image Processing. Dordrecht: Springer Netherlands, 69–76.

Chum, O., Philbin, J., and Zisserman, A., 2008. Near duplicate image detection: min–Hash and tf–idf Weighting. In: Bmvc, 810: 812–815.

Cortes, C., and Vapnik, V., 1995. Support-vector networks, Machine learning, 20(3): 273–297.

Cucchiara, R., Grana, C., Piccardi, M., Prati, A., and Sirotti S., 2001. Improving shadow suppression in moving object detection with HSV color information. In: 2001 IEEE Intelligent Transportation Systems. Proceedings (Cat. No.01TH8585), 25–29 Aug. 2001.

Cusano, C., Ciocca, G., and Schettini, R., 2003. Image annotation using SVM. In: Internet imaging V. International society for optics and photonics, 5304: 330–338.

Gonzalez, R.C., and Woods, R. E., 2008. Digital Image Processing (3rd ed.). Upper Saddle River, NJ, USA: Pearson prentice hall, 657–661.

Gu, P., Zhong, L., Zhang, G. D., Song, S. C., Tang F., Ling M. Q., Gao, L. Z., 2018. The Division of the Late Ediacaran-Cambrian boundary interval stratigraphy and new options of index fossil FAD in South China. Acta Geologica Sinica, 92 (3): 449–465 (in Chinese with English abstract).

Han, J., Kubota, S., Li, G.X., Yao, X.Y., Yang, X.G., Shu, D.G., Li, Y., Kinoshita, S., Sasaki, O., Komiya, T., and Yan, G.,

2013. Early Cambrian pentamerous cubozoan embryos from South China. PLoS One, 8(8), e70741.
Han, J., Li, G.X., Kubota, S., Ou, Q., Toshino, S., Wang, X., Yang, X.G., Uesugi, K., Masato, H., Sasaki, O., Kano, H., Sato, Y., and Komiya, T., 2016. Internal microanatomy and zoological affinity of the early Cambrian *Olivooides*. Acta Geologica Sinica (English Edition), 90(1): 38–65.
Han, J., Cai, Y.P., Schiffbauer, J.D., Hua, H., Wang, X., Yang, X.G., Uesugi, K., Komiya, T., and Sun, J., 2017a. A *Cloudina* –like fossil with evidence of asexual reproduction from the lowest Cambrian, South China. Geological Magazine, 154 (6): 1294–1305.
Han, J., Morris, S.C., Ou, Q., Shu, D.G., and Huang, H., 2017b. Meiofaunal deuterostomes from the basal Cambrian of Shaanxi (China). Nature 542 (7640):228–231.
Haris, K., Efstratiadis, S.N., Maglaveras, N., and Katsaggelos, A.K., 1998. Hybrid image segmentation using watersheds and fast region merging. IEEE Transactions on Image Processing ,7(12): 1684–1699.
Lee, D., and Lee, J., 2007. Domain described support vector classifier for multi-classification problems. Pattern Recognition, 40(1): 41–51.
Lindeberg, T., 2012. Scale invariant feature transform. Scholarpedia, 7(5): 10491.
Liu, Y.H., Shao, T.Q., Zhang, H.Q, Wang, Q., Zhang, Y., Chen, C., Liang, Y., and Xue, J.Q., 2017. A new scyphozoan from the Cambrian Fortunian Stage of South China. Palaeontology, 60(4): 511–518.
Liu, Y.H., Li, Y., Shao, T.Q., Hu, H., Bai, J., Zhang, W.J., Ren, M., and Duan, S.S., 2014. The new record of phosphatized *Cambricodium* fossils from the basal Cambrian of the Southern Shaanxi, China. Acta Micropalaeontologica Sinica, 31(1): 98–103 (in Chinese with English abstract).
Malik, J., Belongie, S., Leung, T., and Shi, J., 2001. Contour and texture analysis for image segmentation. International Journal of Computer Vision, 43(1): 7–27.
Mortensen, E.N., Hongli, D., and Shapiro, L., 2005. A SIFT descriptor with global context. Paper read at 2005 IEEE Computer Society Conference on Computer Vision and Pattern Recognition (CVPR'05), 20–25 June 2005.
Peng, S.C., Babcock, L.E., and Cooper, R.A., 2012. The Cambrian Period. In: Gradstein, F.M., Ogg, J.G., Schmitz, M., and Ogg, G. (eds.), Geological Time Scale 2012. Oxford: Elsevier, 437–488.
Qian, Y., 1977. Hyolitha and some problematica from the Lower Cambrian Meishucun Stage in central and SW China. Acta Palaeontologica Sinica, 16(2): 255–275 (in Chinese with English abstract).
Steiner, M., Li, G.X., Qian, Y., and Zhu, M.Y., 2004a. Lower Cambrian Small Shelly Fossils of northern Sichuan and southern Shaanxi (China), and their biostratigraphic importance. Geobios, 37(2): 259–275.
Steiner, M., Zhu, M.Y., Li, G.X., Qian, Y., and Erdtmann, B.D., 2004b. New early Cambrian bilaterian embryos and larvae from China. Geology, 32(10): 833–836.
Steiner, M., Li, G.X., Qian, Y., Zhu, M.Y., and Erdtmann, B.D., 2007. Neoproterozoic to early Cambrian small shelly fossil assemblages and a revised biostratigraphic correlation of the Yangtze Platform (China). Palaeogeography, Palaeoclimatology, Palaeoecology, 254: 67–99.
Steiner, M., Qian, Y., Li, G.X., Hagadorn, J.W., and Zhu, M.Y., 2014. The developmental cycles of early Cambrian Olivooidae fam. nov. (?Cycloneuralia) from the Yangtze Platform (China). Palaeogeography, Palaeoclimatology, Palaeoecology, 398: 97–124.
Sural, S., Gang, Q., and Pramanik, S., 2002. Segmentation and histogram generation using the HSV color space for image retrieval. In: International Conference on Image Processing, 2, II–II.
Süsstrunk, S., Buckley, R., and Swen, S., 1999. Standard RGB Color Spaces. In: Color and Imaging Conference, Society for Imaging Science and Technology, (1): 127–134.
Vincent, L., 1993. Morphological grayscale reconstruction in image analysis: applications and efficient algorithms. IEEE Transactions on Image Processing, 2(2): 176–201.
Wagstaff, K., Cardie, C., Rogers, S., and Schrödl, S., 2001. Constrained K–means Clustering with Background Knowledge. In: Eighteenth International Conference on Machine Learning, 1: 577–584.
Yang, X. G., Wang, X., Han, J., Schiffbauer, J. D., Uesugi, K., Sasaki, O., and Komiya, T., 2017. Euendoliths versus ambient inclusion trails from early Cambrian Kuanchuanpu Formation, South China. Palaeogeography, Palaeoclimatology, Palaeoecology, 476: 147–157.
Yang, X.G., and Han, J., 2017. Ambient inclusion trails and microboring structures on Early Cambrian microfossils. Chinese Science Bulletin, 62(35): 4179–4188 (in Chinese with English abstract).
Zhang, H.Q., and Dong, X.P., 2015. The oldest known larva and its implications for the plesiomorphy of metazoan development. Science Bulletin, 60(22): 1947–1953.
Zhang, H.Q., Xiao, S., Liu, Y.H., Yuan, X.L., Wan, B., Muscente, A.D., Shao, T.Q, Gong, H., and Cao, G.H., 2015. Armored kinorhynch-like scalidophoran animals from the early Cambrian. Scientific reports 5.
Zhang, J., Hao, X., Hu, Y., Yang, X.G, Wang, X., Yao, X.Y., Shen, Y., and Han J., 2017. A spherical hat–shaped organism from the Lower Cambrian Kuanchuanpu Formation. Acta Palaeontologica Sinica, 56(4): 415–424 (in Chinese with English abstract).
Zhang, T., Lei, D.B., Wang, B., Niu, B., Yang, X.G., and Han, J., 2019. Artificial intelligence identification of microfossils from the Lower Cambrian Kuchuanpu Formation in southern Shaanxi, China. Acta Paalaeontologica Sinica, 58(2) (in Chinese with English abstract).
Zheng, Y.J., Yao, X.Y., Han, J., and Guo, J.F., 2017. Microscopic fossils with multi-level tetrad cell structures from the Cambrian Kuanchuanpu Formation in south Shaanxi. Acta Palaeontologica Sinica, 56(4): 440–448 (in Chinese with English abstract).

About the first author

ZHANG Tao, male, born in 1980 in Dali, Shaanxi Province. Doctor, lecturer in Northwest University. He is now interested in the study on Electrical Engineering and artificial intelligence. E-mail: zhangtao129 @nwu.edu.cn; phone:13772091231.

About the corresponding authors

YANG Xiaoguang, male, born in 1987 in Wuchang, Heilongjiang Province. Doctor, post-doctoral researcher in Northwest University, with research interests in the early Cambrian microfossils. E-mail: lqzy 0301@gmail.com; phone: 15667070061.

WANG Bin, male, born in 1979 in Longyao, Hebei Province. Doctor, lecturer in Northwest University. His major research interests are computer vision and AI processing of big data. E-mail: wbin@nwu.edu.cn; phone: 13572802306.